SAND--90-2909C

DE91 004506

FLOW BEHAVIOR OF Ti-24Al-11Nb AT HIGH STRAIN RATES

L. S. Harbison+, R.J. Bourcier,°, and D.A. Koss+

+Department of Materials Science and Engineering
Penn State University
University Park, PA 16802

°Sandia National Laboratories
P.O. Box 5800
Albuquerque, NM 87185

ABSTRACT

The deformation and crack initiation behavior of Ti-24Al-11Nb has been examined over a temperature range of 298 to 923 K and for strain rates from 10^{-4}/s to 10^{2}/s. Tests performed in compression indicate much lower strain hardening at 10^{2}/s than at either 10^{-1}/s or 10^{-4}/s at all temperatures. Associated with this behavior is the occurrence of non-uniform, localized deformation bands at 10^{2}/s. An analysis indicates that adiabatic deformation conditions predominate at 10^{2}/s and that these result in adiabatic softening. Furthermore, as a result of non-uniform deformation and adiabatic heating, this Ti_3-Al-based alloy is actually more resistant to strain-induced microcrack initiation at 10^{2}/s than at 10^{-4}/s during room temperature testing.

INTRODUCTION

Titanium aluminide alloys based on Ti_3Al have been the subject of extensive alloy development as well as fundamental research. As a result, there have been a number of studies which have examined the deformation and fracture behavior of Ti_3Al-based alloys over a wide range of microstructures and temperatures; see ref's [1-3] for reviews. However, there has been no study of the deformation behavior of these materials at high strain rates. This is despite the fact that conventional alpha-beta titanium alloys are known to be very susceptible to adiabatic shear localizaton at large plastic strains and high strain rates [4-8]. While the deformation behavior and associated mechanisms of the Ti_3Al alloys at low strain rates clearly differ from those of alpha-beta alloys, there are also similarities [1]. Thus, the purpose of this research is to examine the

deformation behavior of a Ti_3Al-based alloy over ranges of strain-rates (10^{-4}/s to 10^{2}/s) and temperatures (298 to 923 K). The alloy Ti-24Al-11Nb(at.%) was chosen as a model system. Particular attention is given to evidence of adiabatic deformation, and associated with it, flow localization at high strain rates. An interesting and unexpected effect of strain rate on strain-induced microcracking is also presented.

EXPERIMENTAL PROCEDURE

The titanium aluminide alloy used in this study was in the form of 12.7 mm rolled plate. In terms of major elements, the composition of the Ti_3Al-based alloy (in atomic percentages) was Ti-24%Al-11%Nb (hereafter referred to as Ti-24-11); detailed chemical analysis of the alloy is given in Table 1. After specimen preparation, all Ti-24-11 samples were heat treated at 1033K for one hour in a vacuum of 2×10^{-4} Pa Torr followed by a helium gas quench.

Table 1: Chemical Analysis of the Ti-24-11 Alloy in Weight Percentage

ALLOY	Al	Nb	C	Fe	N	H	O
Ti-24-11	14.5	21.6	0.017	0.05	0.013	0.007	0.110

Uniaxial compression testing of the Ti-24-11 was performed at strain-rates from 10^{-4} to 10^{2}/s and temperatures from 298 to 923 K. Two specimen geometries were used. Rectangular specimens (12.7 x 6.35 x 6.35 mm) were used for the purpose of monitoring surface cracking and/or relief which occurs during the tests. Cylindrical specimens (12.7 x 6.35 mm diameter) were used for high strain-rate testing. All specimens had a similar through-thickness orientation with respect to the plate thickness. Prior to compression testing one side face of each rectangular specimen was polished through 0.05 μm alumina for subsequent optical and scanning electron microscopy observations.

Tests at low strain-rates (initial strain rates of 10^{-4}/s) were completed on an Instron Model 4206 screw-driven universal testing machine. Tests were performed over the range of

temperatures 298 to 923 K; for temperatures ≥ 773K, tests were performed in high purity flowing argon to minimize oxygen contamination. High strain-rate testing (initial strain-rates from 10^{-1} to 10^{2}/s) was performed on an MTS model 458 servohydraulic high rate testing system in conjunction with a four-post cage-type fixture of 4340 steel. Mechanical stops of T15 tool steel were placed around the four sliding posts of the basket fixture to limit the amount of strain imposed on the test specimens during testing at 10^{2}/s. Data for the 10^{2}/s tests was recorded using a moving point average smoothing program to eliminate elastic fixture ringing. Brass shear pins were employed to allow the fixture to be pulled at the desired displacement rate without the need to slow the fixture down to obtain the desired final specimen strain. In order to verify the machine behavior at 10^{2}/s, a series of compression tests were performed on 304 stainless steel over a range of strain rates from 10^{-4} to 10^{2}/s. Those data duplicated earlier results of Stout and Follansbee [9], indicating that the tests at 10^{2}/s yielded valid data.

EXPERIMENTAL RESULTS

A. Microstructure

An examination of the Ti-24-11 microstructures as shown in Fig. 1 suggest a two-phase microstructure consisting of equiaxed alpha-two grains (approximately 10 μm in size) with discontinuous beta phase present at alpha-two grain boundaries and triple points. Using backscatter electron imaging, Fig. 1a reveals that there is considerable compositional variation within the alloy, resulting in local differences in beta-phase content, as well as within the alpha-two grains, resulting from differences in the spatial distribution of Al and Nb. A TEM examination of this alloy [10] reveals the presence of ordered beta, alpha-two, and a relatively large amount of orthorhomic phase. In some regions, entire grains appear to have orthorhombic structures while in others the orthorhombic phase was located only in the vicinity of the Nb-rich beta phase[10], as expected [11,12].

Another significant aspect of the microstructure was the presence of faint "bands" evident in Fig. 1c in the as-rolled condition. The alpha-two grains within these bands appear elongated, suggesting non-uniform deformation through the plate thickness during hot rolling.

B. Stress-Strain Response

The compressive stress-strain response of the Ti-24-11 alloy over a range of temperatures is shown in Figs 2 and 3 for strain rates of 10^{-4} and 10^{2}/s, respectively. Although those data are not presented here, the stress-strain response at 10^{-1}/s are nearly identical to those at 10^{-4}/s. The strain-hardening exponents have been computed for the data in Fig. 2 according to the Ludwik equation $\sigma = \sigma_0 + k\varepsilon^n$ where σ_0 is the yield stress, k is a strength coefficient and n is the strain hardening coefficient. As shown in Table II, and as is evident in Fig's 2 and 3, the n-values at 10^{-4}/s are relatively independent of temperature over the range 298 to 923K. It is interesting to note that the same Ti-24-11 alloy with a basket weave alpha-two phase plus beta microstructure exhibits a significantly lower n-value at 10^{-4}/s than the present equiaxed structure. Specifically, n = 0.44 in the basketweave condition (vs. 0.94 observed here) at 298K and 0.51 vs 0.93 presently observed at 773K [13].

Table II: Strain Hardening Exponents for Ti-24-11 as a Function of Temperature and Strain Rates. Note: the n-value is based on $\sigma = \sigma_0 + k\varepsilon^n$.

	298	448	623	773	923K
n @ 10^{-4}/s	0.94	1.16	0.99	1.01	0.94
n @ 10^{-1}/s	1.09	1.07	1.09		0.95
n @ 10^{2}/s	0.44	0.61	0.70		0.66

Of particular interest in this study is the stress-strain behavior of the Ti-24-11 at 10^{2}/s as shown in Fig. 3. When compared to that at 10^{-4}/s (Fig. 2), the flow behavior at 10^{2}/s is characterized by an expected increase in yield strength. However, somewhat unexpectedly, the stress-response at 10^{2}/s exhibits a much lower apparent rate of strain hardening at $\varepsilon \geq 0.01$ than at

either 10^{-1}/s or 10^{-4}/s. This is shown more clearly in Fig. 4. Thus as listed in Table II, the n-values derived from the σ-ε data at 10^{2}/s are consistently lower than at either 10^{-1}/s or 10^{-4}/s. While this effect is observed at all test temperatures between 298 and 773K, it is most pronounced at 298K as is shown in Fig. 4.

Finally, it might be noted that in all cases, the strain-rate hardening exponent ($m=d\ln\sigma/d\ln\dot{\varepsilon}$) was small ($m \leq 0.01$) even at temperatures to 923K. This is consistent with the temperature dependence of the yield stress, see Fig. 5, which shows the yield stress to be sensitive to temperature, decreasing continuously with increasing temperature at all strain rates.

C. Microcracking Behavior

As shown in Fig. 6, backscattered SEM micrographs show that while extensive microcracking occurs on the surface of the compression specimens deformed 0.08 strain at 10^{-4}/s and 298K, no cracking is evident at 10^{-4}/s and 448K or at 10^{2}/s and both 298K and 448K. Thus at 10^{-4}/s there is a transition from extensive microcracking at room temperature to no microcracking at 448K. This occurs despite only a small difference in stress-strain response; the 448K flow stresses are decreased about 15% but the same strain-hardening behavior prevails as shown in Fig. 2. In addition to the onset of microcracking being sensitive to temperature, it is also sensitive to strain rate. Fig. 6 shows that, quite surprisingly, the Ti-24-11 exhibits no microcracks when deformed at 10^{2}/s at 298K even though it cracks profusely at 10^{-4}/s (compare Fig. 6a to 6c).

In all cases, extensive surface relief and coarse slip offsets are observed due to strain incompatibilities between adjacent "alpha-two" grains; this is similar to previous observatons [13]. The orientations of the microcracks are roughly parallel to the compression axis and perpendicular to the maximum principal tensile strain, as expected.

At lower magnifications, SEM micrographs from longitudinal cross sections of the specimen reveal another pertinent feature: flow localization which occurs at 10^{2}/s but not at 10^{-4}/s. As seen in Fig. 7a, the regions denoted by the arrows indicate bands of intense deformation or shear bands, causing pronounced local elongations of the equiaxed alpha-two grains. Such flow

localization is observed under all temperature conditions at 10^2/s, but it appears most pronounced at 298K. At 298K, the bands occupy about 10% of the volume of the material at $\varepsilon = 0.08$ and vary in thickness being ≤ 100 μm thick. Also of interest is the appearance of the beta phase with the intense flow bands. Fig. 7b shows that the beta phase, at least on the specimen surface, appears relatively undeformed when compared with the alpha-two phase. There is no evidence of any transformed microstructure.

DISCUSSION

The present study indicates that at strain rates of 10^2/s, the deformation response of Ti-24-11 alloy is different than at either 10^{-4}/s or 10^{-1}/s. Specifically, at 10^2/s there is (a) a pronounced decrease in strain hardening (see Table II or Fig. 4), (b) an ocurrance of zones or bands of intense deformation or "shear" (see Fig. 7), (c) an absence of microcracking which is profuse at room temperature at 10^{-4}/s (see Fig. 6). Furthermore, close examination of stress-strain response over a wide range of temperatures and strain rates indicates that the Ti-24-11 alloy exhibits relatively small strain-rate hardening ($m \cong .01$), a moderate degree of strain hardening at low strain rates which is independent of temperature ($n = d\ln\sigma/d\ln\varepsilon \cong 0.15 - 0.20$ at $10^{-4} \leq \dot{\varepsilon} \leq 10^{-1}$/s and $298 \leq T \leq 923$K), and a significant temperature dependence of the yield and flow stress ($d\sigma/dT$ ranges from -0.85 MPa/K @ 298K to -0.25 MPa/K at 773K).

Adiabatic shear deformation is a flow localization phenomenon which usually occurs in metals deformed at high strain rates to large plastic strains. It is typically characterized by bands of intense deformation distributed between regions of relatively homogeneous deformation. The flow localization process is a result of the destabilizing effect of heat generation caused by local plastic flow which results in thermal softening exceeding the stabilizing effects of strain hardening and strain-rate hardening. Conventional alpha-beta titanium alloys are known to be quite susceptible to the formation of adiabatic shear band formation at high strain rates [4-8]; in some cases, these can be very "severe", resulting in a transformed microstructure [6,13]. We believe that the high rate deformation behavior of the Ti-24-11 in the present study indicates the onset of adiabatic flow

localization in the form of intensity deformed shear bands at 10^2/s. We also propose that it is the formation and development of these shear bands which results in the macroscopic decrease in strain hardening as well as the absence of microcracking observed at 10^2/s.

The above hypothesis is supported by a straight-forward application of the basic concepts of adiabatic deformation and strain localization. First, whether or not adiabatic conditions occur at 10^2/s can be anticipated by an application of a one-dimensional heat flow solution for a constant rate of heat input into a region L wide. The temperature profile at time t depends on the parameter $L^2/k_T t$ where k_T is the thermal diffusivity (note: $k_T = k/\rho Cp$, where k is the thermal conductivity, ρ the density, and Cp the specific heat). For predominantly adiabatic conditions [15].

$$\frac{L^2}{k_T t} > 1 \qquad (1)$$

For the Ti-24-11 alloy in the present study, the width L of the shear bands are less than 100 μm (see Fig. 7), and the time of deformation $t = \varepsilon/\dot{\varepsilon}$ varies from $\cong 1 \times 10^{-4}$s from the onset of the instability at $\varepsilon \simeq .01$ to 8×10^{-4}s at the end of the test ($\varepsilon = 0.08$). The difficulty in evaluating Eq 1 is that the magnitude of k_T for Ti-24-11 is not known. However, an examination of several commercial alpha-beta and beta alloys indicates that both Cp and k are relatively constant and depend only weakly on composition. Thus, assuming Ti-24-11 has similar k and C_p values to Ti-6Al-4V [15] and correcting for the density difference between Ti-6-4 and Ti-24-11, we will assume $k_T \cong 2 \times 10^{-6}$ m^2/s. Under these conditions the magnitude of the term $(L^2/k_T t) \cong 6$ to 50, depending on whether t is taken as the duration of the test or at the onset of the instability, which from the σ-ε response appears to be $\varepsilon \cong 0.01$. In either case, we conclude that deformation of Ti-24-11 at 10^2/s will be predominantly adiabatic since large differences in k and C_p would be required to cause the $(L^2/k_T t)$ term to be less than one. It is also interesting to note that at 10^{-1}/s, $(L^2/k_T t) << 1$ and thus isothermal conditions dominate, as is expected from the stress-strain response.

Given the existence of adiabatic deformation conditions, we now consider its implications with regard to plastic instabilities and adiabatic shear bands. Various analyses have been

performed to predict the critical strains for the onset of a shear instability for a homogeneous material; see, for example, refs [6,15]. For a material whose strain hardening behavior is similar to that of Ti-24-11, the predicted instability strain (> 0.17) are much larger than that ($\varepsilon_o \cong 0.01$) indicated experimentally by the marked decrease in strain hardening; see Fig. 4. We believe that our experimentally observed initiation strain is a result of nonuniformity in the Ti-24-11 plate material. Figure 1c clearly shows the presence of thin bands of elongated "alpha-two" grains in the initial microstructure. It is likely that the flow strength of these local volumes of material is lower than that of the bulk, causing them to be heavily deformed during plate rolling. These bands may act as linear imperfections during the high rate compression tests, triggering the initiation of adiabatic flow instability at a small macroscopic strain level.

Since adiabatic deformation prevails at 10^2/s, the question remains : can it account for the observed σ-ϵ response and lack of room-temperature cracking at 10^2/s? The answer depends on the magnitude of temperature increase caused by local adiabatic heating during plastic deformation. The temperature increase ΔT within the deformation bands is given by expression

$$\Delta T = \frac{\beta}{\rho\, Cp} \int \frac{\sigma d\varepsilon}{\phi} \qquad (2)$$

where $\beta \cong 0.9$ is assumed to be the fraction of plastic deformation converted into heat, ρ Cp is approximately 2.44 MPa/K if we assume Cp for Ti-24-11 is roughly equal to that of Ti-6Al-4V. In Eq. 2, the term ϕ is our modification to account for the fraction of material deforming if adiabatic shear bands dominate deformation after an initation strain ε_o. We anticipate that the value of parameter ϕ varies from 1.0 initially to approximately 0.1 at $\varepsilon > \varepsilon_o$, after which slip is confined primarily to shear bands occupying about 10 vol % of the specimen. Assuming a $\varepsilon_o \cong 0.01$ (see above) and that ϕ has a value of 0.1 from $0.01 \leq \varepsilon \leq .08$, we estimate that the temperature within the shear bands is about 230K higher than the matrix at a macroscopic strain of 0.08 for a room temperature test.

Using such information, it is possible to calculate an "isothermal" stress-strain response for Ti-24-11 at 10^2/s. For example, given the temperature dependence of the yield stress in Fig. 6, an

increase of 230K from 300K to 530K would decrease the flow stress approximately 150 MPa at $\varepsilon = 0.08$. Using such an analysis we can compute the "isothermal" 10^2/s σ–ε response based on Eq (2) and the σ-T data in Fig. 6, assuming the plastic flow instability initiates at $\varepsilon = 0.01$. Fig. 4 shows that the predicted "isothermal" stress-strain response at 10^2/s indicates "normal" strain hardening and a reasonable increase in flow stress due to strain-rate hardening, supporting our analysis.

The presence of significant adiabatic heating and the development of localized deformation bands is also consistent with the absence of microcracking at 10^2/s at room temperature. Results at 10^{-4}/s shown in Fig. 6 indicate that an increase of the test temperature to 175K is sufficient to suppress microcracking. At 10^2/s and 300K, we speculate that (a) the local strains ($\varepsilon = 0.01$ - 0.02) outside the shear bands were too small to initiate cracks in compression at room temperature and (b) the large strains ($\varepsilon \cong 0.5$ to 0.7) which occurred within bands did so at temperatures > 200K above room temperature. At these temperatures, the material is quite resistant to microcracking, as seen in Fig. 6.

Finally it is interesting to note that even though the macroscopic flow response of Ti-24-11 is governed predominantly by the "alpha-two" phase, the bcc beta is likely to be much harder at high strain rates during room temperature deformation. This can be deduced from thermally activated rate analysis [8] and from the strong temperature dependence of the yield stress of the beta phase [16]. As a result, within the shear bands, a relatively softer alpha-two and/or O-phase appears to flow easily around beta particles, leaving them comparatively equiaxed; see Fig. 7b.

SUMMARY

The compressive stress-strain response of Ti-24-11 has been investigated over a range of strain rates from 10^{-4}/s to 10^2/s and temperatures from 298K to 923K. The data show that the apparent strain hardening at 10^2/s is much lower than at either 10^{-4}/s or 10^{-1}/s. Accompanying this response is the presence of non-uniform localized deformation bands which form at 10^2/s. An analysis indicates that adiabatic deformation conditions are satisfied at 10^2/s but not at 10^{-1}/s or

10^{-4}/s. Furthermore, the pre-existing planar imperfections within the microstructure appear to trigger flow instabilities at strains as small as $\varepsilon = 0.01$. Most of the ensuing strain occurs within bands which occupy only ≈10% of the volume of the specimen. The calculated increases in temperatures within the localized bands of deformation can account for the observed decrease in macroscopic strain hardening as well as the observed increased resistance to strain-induced microcracking at high strain rates.

ACKNOWLEDGEMENTS

The assistance of D. Schmale is gratefully acknowledged. This research was supported by Sandia National Laboratories through Contract No. 06-9583 and by the U. S. Department of Energy under Contract NO. DE-AC04-76DP00789.

REFERENCES

1. D. A. Koss, D. Banerjee, D. A. Lukasak and A. K. Gogia, in High Temperature Aluminides and Intermetallics, S. H. Whang, C. T. Liu, D. Pope, and J. Stiegler, (eds.), TMS, Warrendale, 1990, p. 175.
2. R. G. Rowe, in High Temperature Aluminides and Intermetallics, S. H. Whang, C. T. Liu, D. Pope, and J. Stiegler, (eds.), TMS, Warrendale, 1990, p. 375.
3. Y-W. Kim and F. H. Froes, in High Temperature Aluminides and Intermetallics, S. H. Whang, C. T. Liu, D. Pope, and J. Stiegler, (eds.), TMS, Warrendale, 1990, p. 465.
4. R. F. Recht, J. Appl. Mech. Trans. ASME, 31 (1964) 189.
5. R. S. Culver, in Metallurgical Effects at High Strain Rates, R. W. Rohde, B. M. Butcher, J. R. Holland, and C. H. Karnes (eds.), Plenum Press, New York, 1973, p. 519.
6. S. P. Timothy and I. M. Hutchings, Acta Metall, 33 (1985), 667.
7. H. Grebe, H. Pak, and M. A. Myers, Metall. Trans. A, 17A (1985), 761.
8. P. S. Follansbee and G. T. Gray III, Metall. Trans. A, 20A (1989), 863.
9. M. G. Stout and P. S. Follansbee, Trans ASME, 108 (1986), 344.
10. A. S. Akkurt and G. M. Bond, unpublished research, 1990.
11. A. K. Gogia, D. Banerjee, and T. K. Nandy, Metall. Trans. A 21A (1990), 609.

12. D. Banerjee, A. K. Gogia, T. K. Nandi, and V. A. Joshi, Acta Metall, 36 (1988), 871.

13. D. M. Lukasak and D. A. Koss, Metall Trans. A, 21A (1990), 135.

14. S. P. Timothy, Acta Metall, 35 (1987), 301.

15. G. B. Olson , J. F. Mescall, and M. Arizio, in Shock Waves and HIgh Strain-Rate Phenomena in Metals, Plenum Press, New York, 1981, p. 221.

16. S. J. Gittis and D. A. Koss, in High Temperature Ordered Intermetallic Alloys III, C. T. Liu, A. J. Taub, N. S. Stoloff, and C. C. Koch (eds.), MRS, Pittsburgh, 1989, p. 323.

LIST OF FIGURES

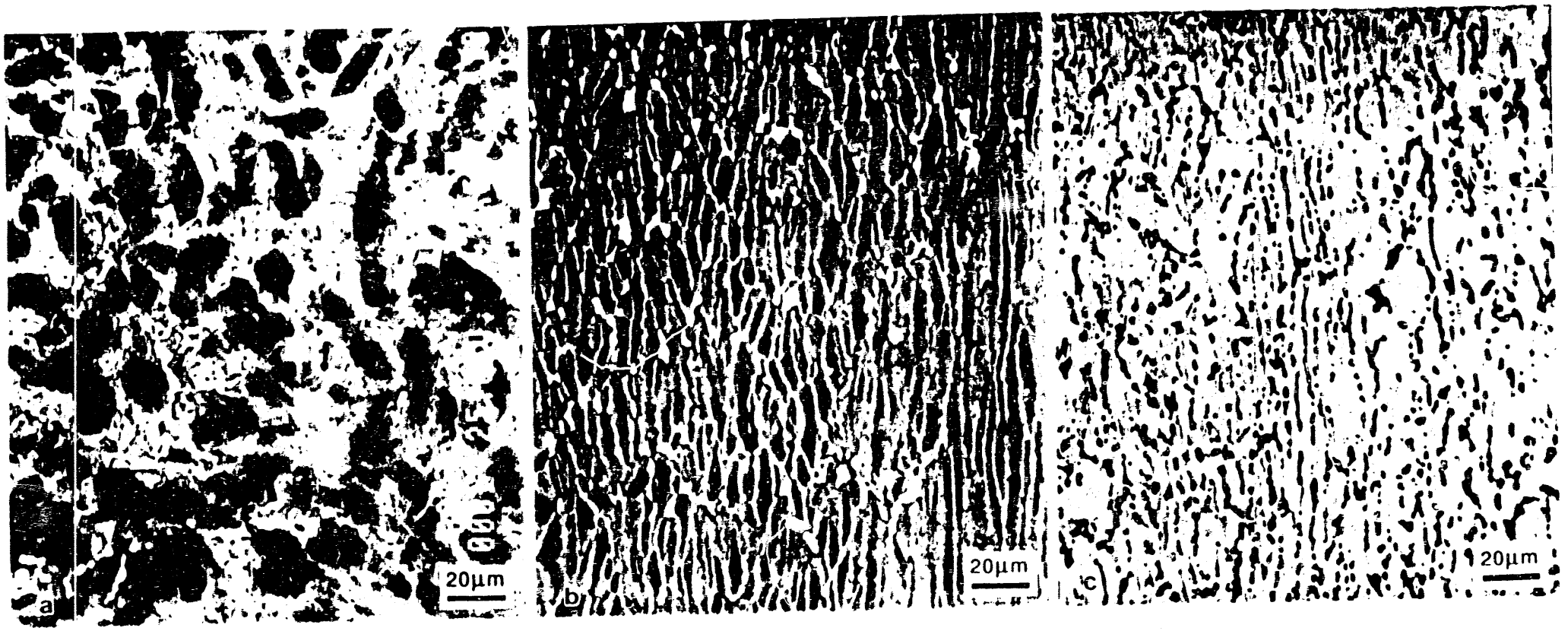

Fig. 1. Microstructures of the Ti-24-11 test specimens: (a) and (b) back-scatter SEM images, and (c) optical microscopy.

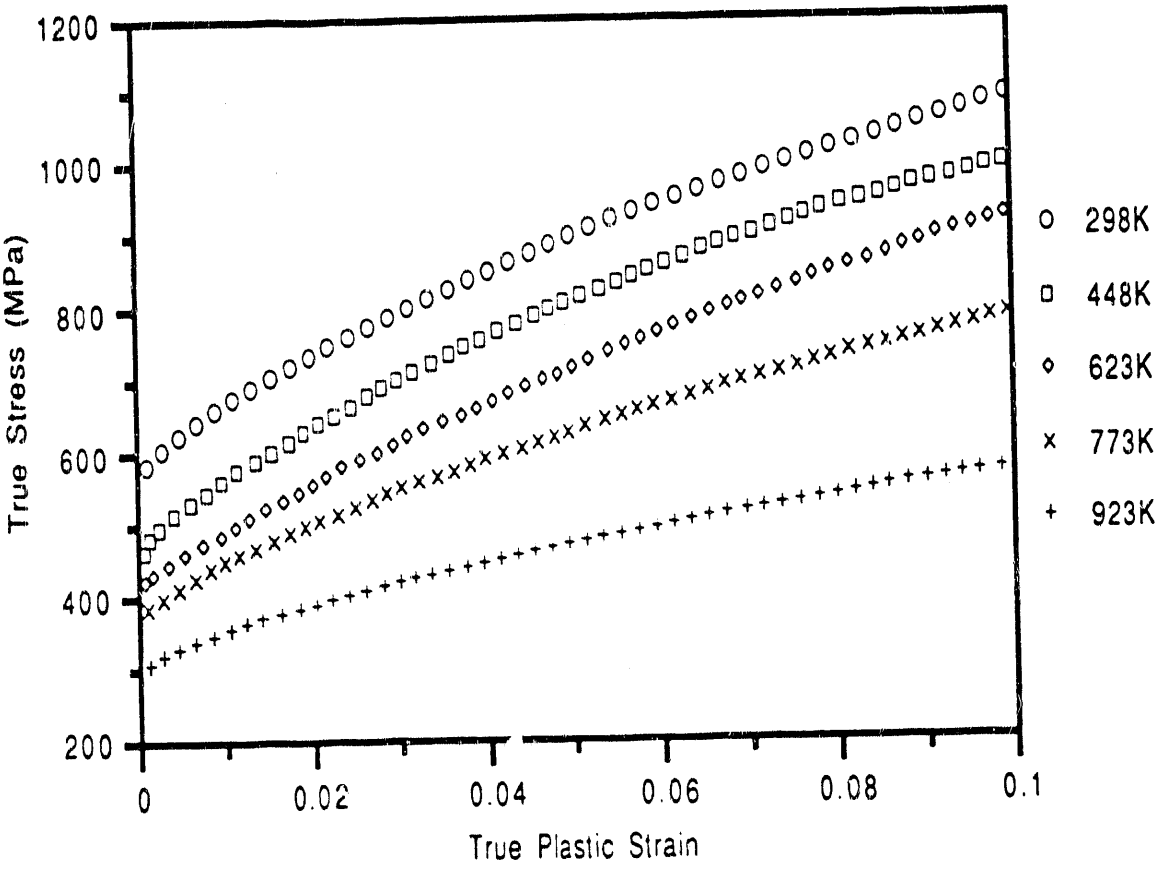

Fig. 2. True stress-true strain behavior of Ti-24-11 in compression at initial strain rates of 10^{-4}/s.

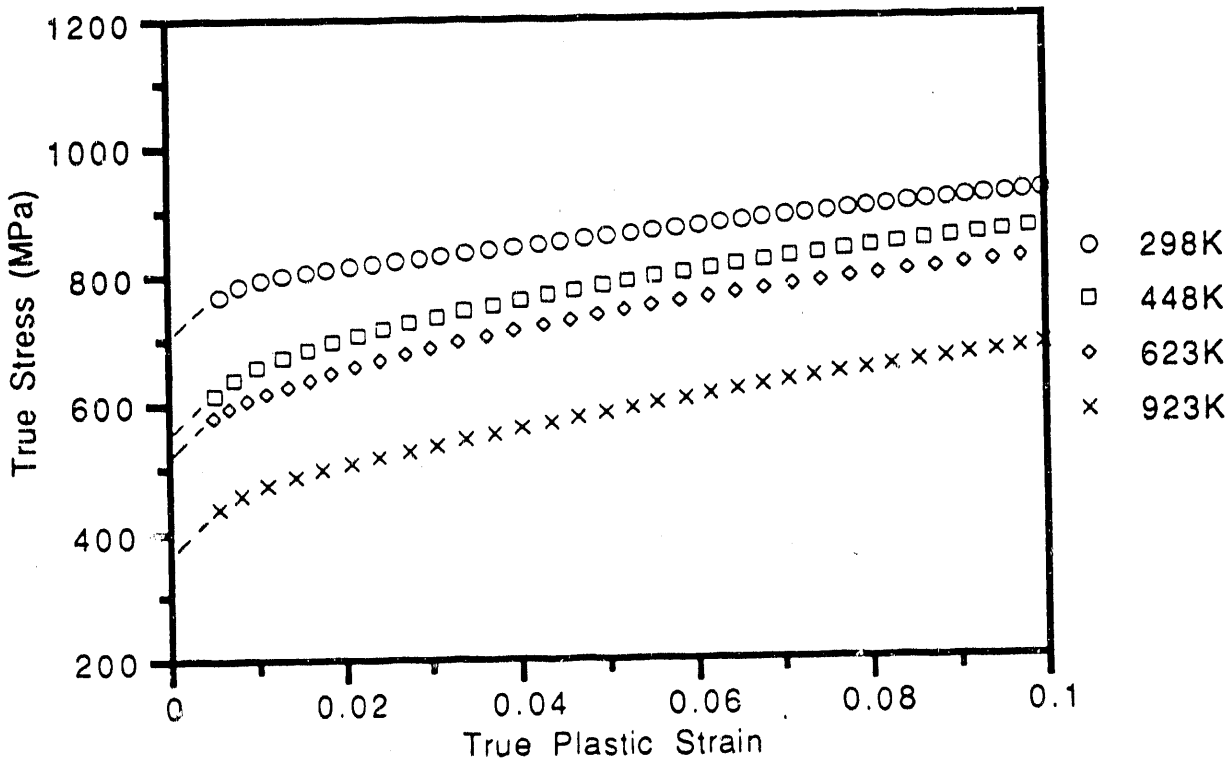

Fig. 3. True stress-true strain behavior of Ti-24-11 in compression at initial strain rates of 10^{-2}/s.

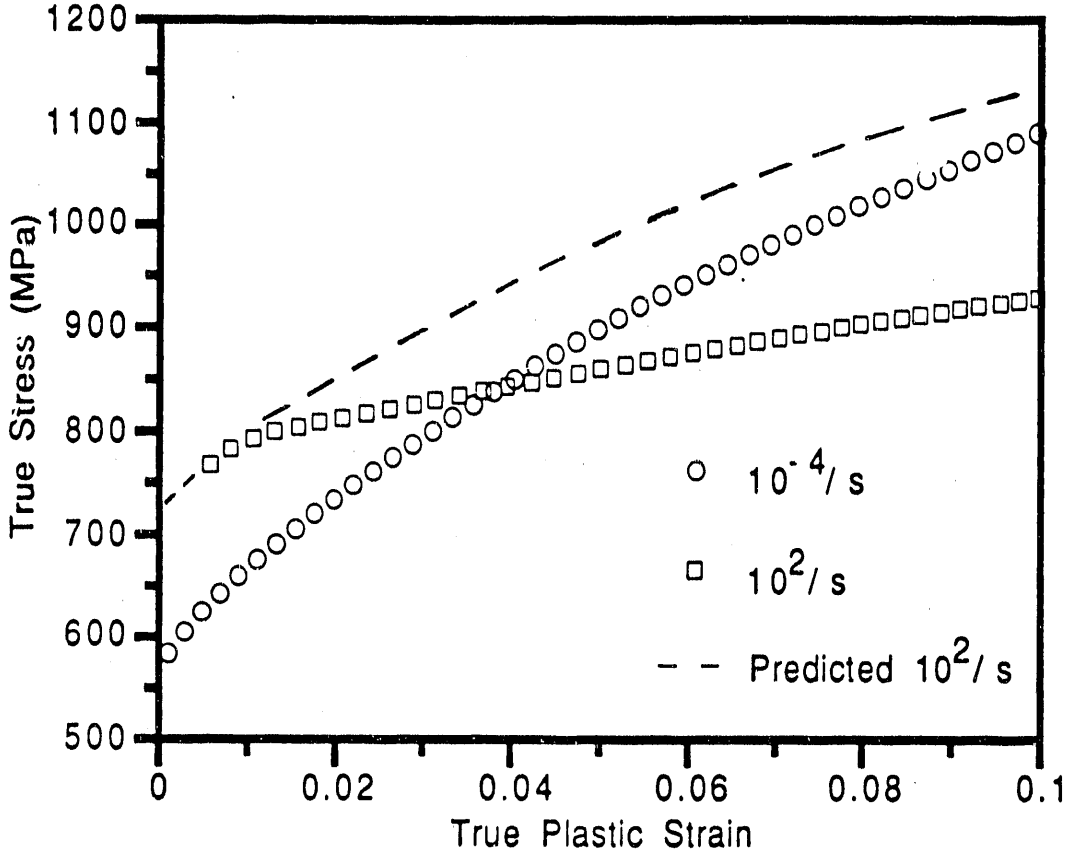

Fig. 4. A comparison of room temperature compressive stress-strain responses at 10^{-4}/s. 10^{-1}/s and 10^{+2}/s. The predicated curve is based on an analysis assuming adiabatic flow (see discussion).

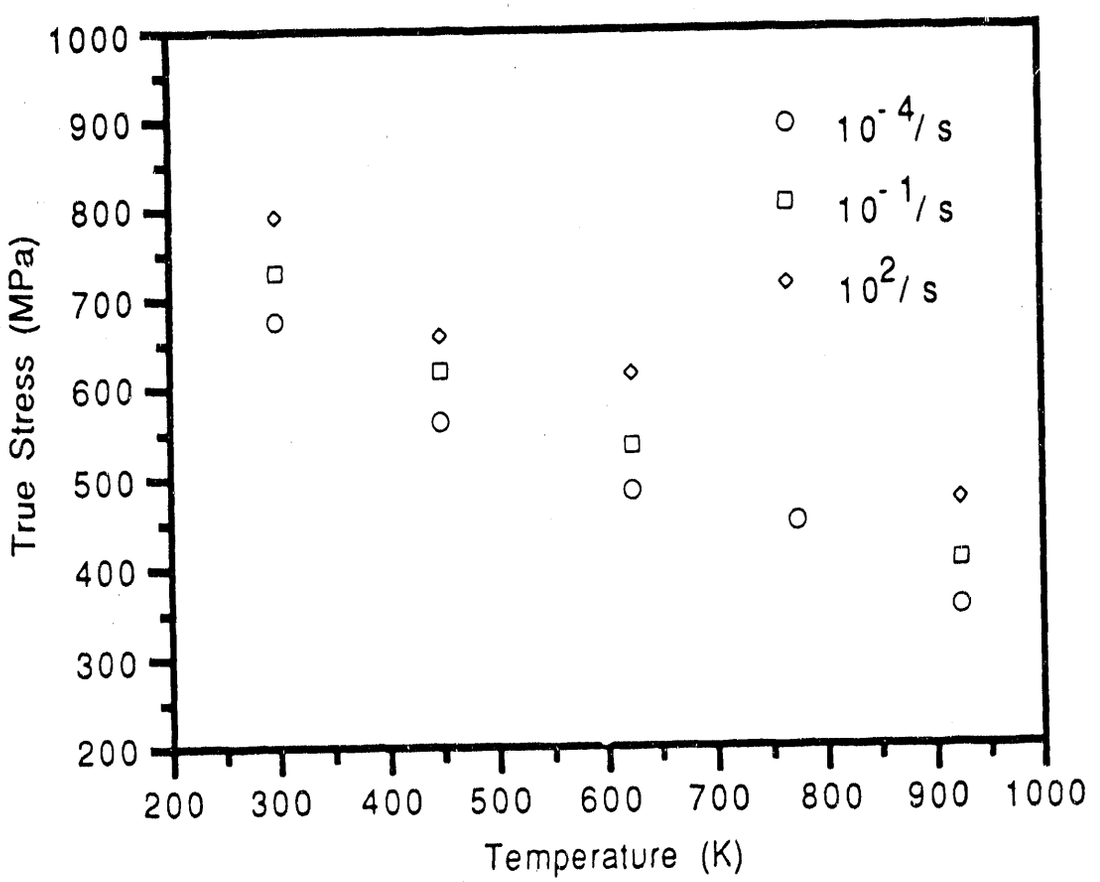

Fig. 5. The temperature dependence of the flow stress of Ti-24-11 at 0.01 strain as a function of strain rate.

Fig. 6. Backscattered SEM micrographs showing microcracking, slip, and surface relief after 0.08 compressive strain under the strain-rate/temperature conditions noted.

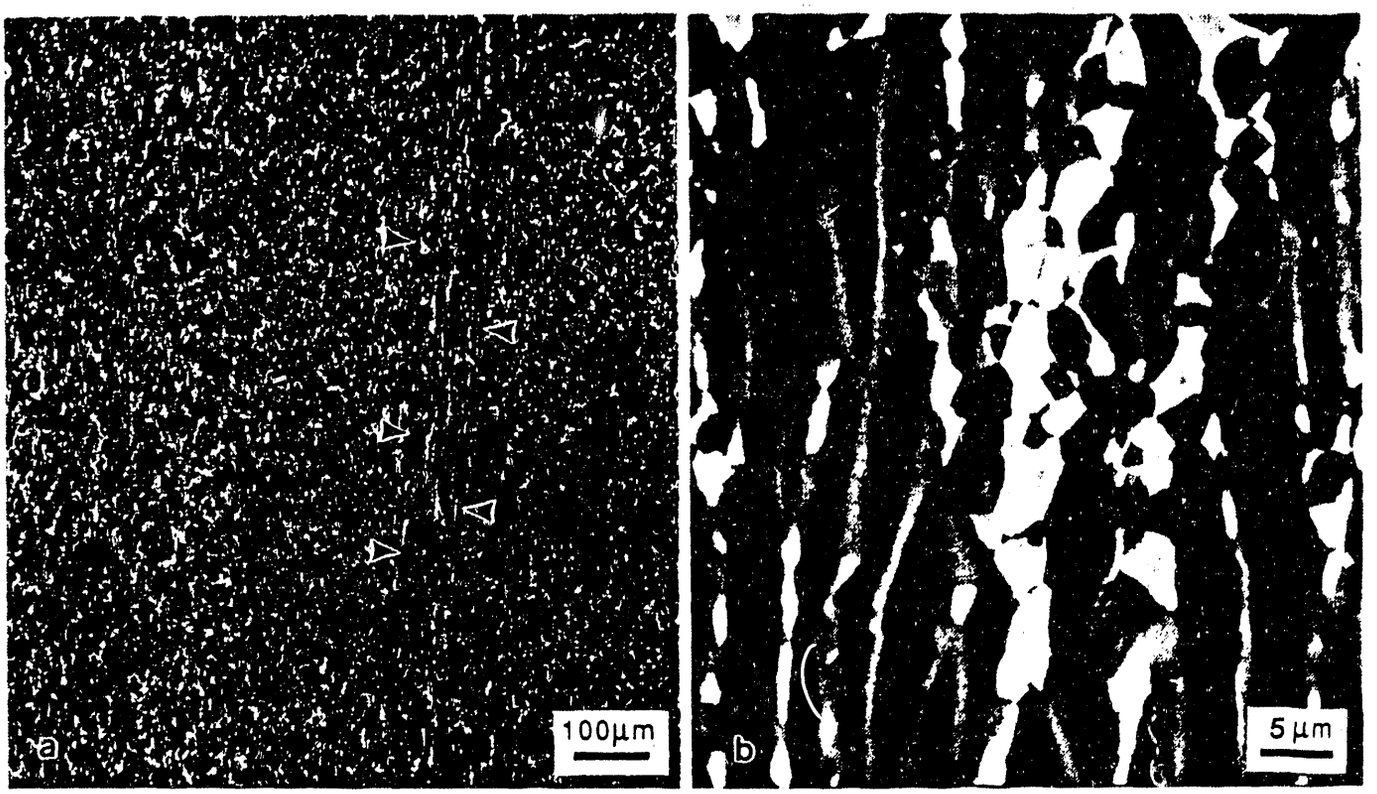

Fig. 7. SEM micrographs showing flow localization in Ti-24-11 after 0.08 strain at 10^2/s and 298K.

END

DATE FILMED

12/18/90